Noise Characterization and Emulation for Low-Voltage Power Line Channels between 150 kHz and 10 MHz

by Bin Han, Vlad Stoica, Cornelius Kalser,

Nico Otterbach, Klaus Dostert
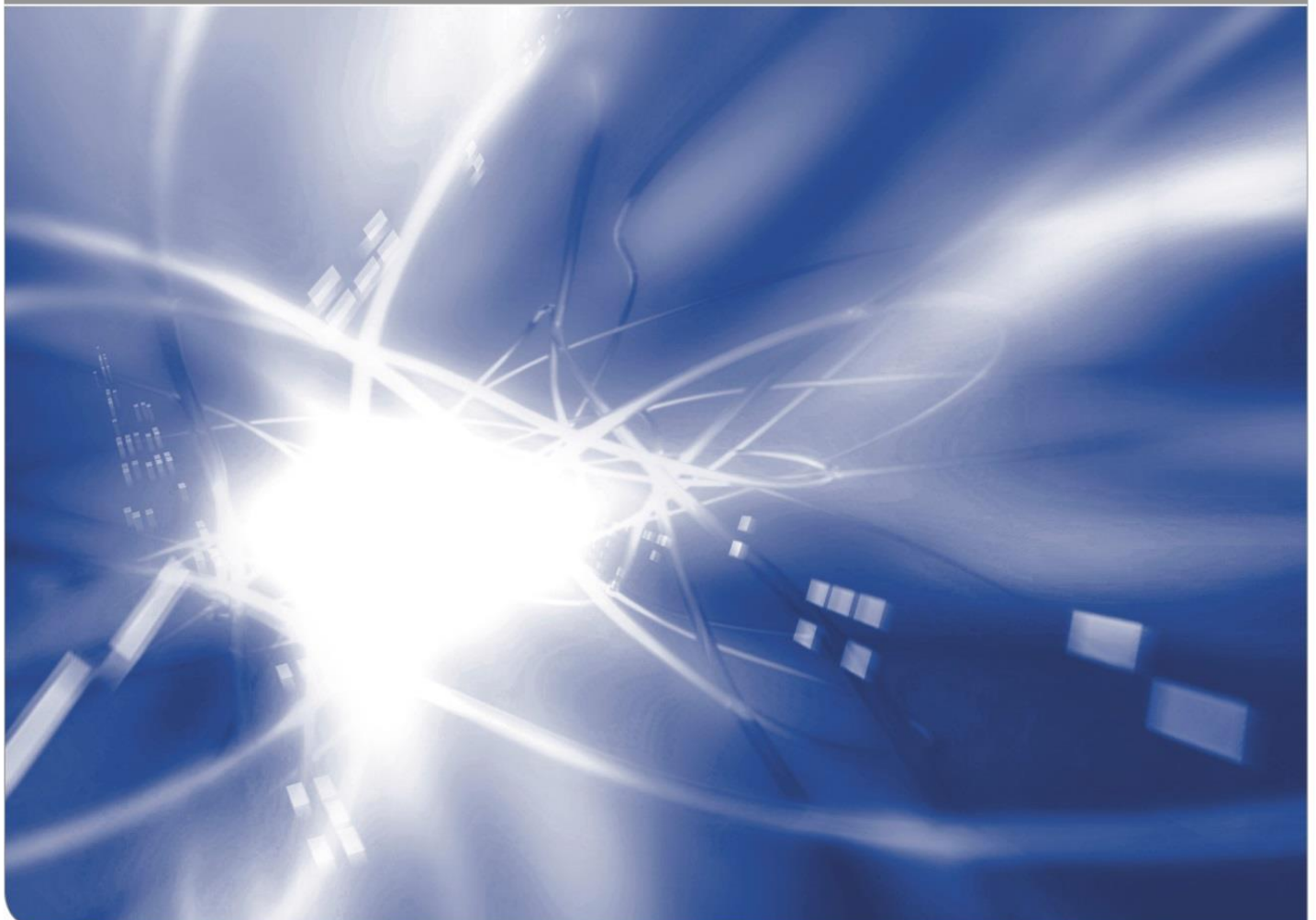
Noise Characterization and Emulation for Low-Voltage Power Line Channels between 150 kHz and 10 MHz

Bin Han, Vlad Stoica, Cornelius Kaiser, Nico Otterbach, and Klaus Dostert, *Senior Member, IEEE*

Abstract—**Characterization and emulation of power line noise have attracted interest since long, in both narrowband and broadband applications. Based on existing models, this paper presents a systematic approach to extract and parameterize each subtype of low-voltage (LV) power line noise between 150 kHz and 10 MHz. Based on the characterization, a FPGA-based emulator is proposed to emulate power line noise scenarios flexibly. A LV power line noise measuring platform is also presented with sample measurements and their emulation.**

Index Terms—**Power line communications, PLC, noise characterization, emulation**

I. INTRODUCTION

Power line communication (PLC), due to its unique advantage of using the widely existing power line infrastructure, has been considered as a competitive solution for communications in smart grid, and has thus raised a lot of interest in the past decade. However, the existing power lines were not originally designed for data transmission, but only for energy delivery. They transmit information inferiorly due to their high attenuation and low electromagnetic compatibilities (EMC).

Existing PLC technologies are usually divided into narrowband (NB) and broadband (BB). Generally, NB-PLC systems work in the frequency band below 500 kHz, whereas BB-PLC systems make use of the wide band above 2 MHz [1]. Since the 1990s, many researchers have made efforts to characterize the behaviors of power line channels in both narrowband and broadband, especially on the low-voltage (LV) level, including the access domain and the indoor domain [2]–[6]. Nowadays, it is generally agreed that the power line channels suffer from time-varying frequency-selective fading and adverse noise scenarios [7]. Besides, both the channel transfer function (CTF) and the noise scenario are dependent on the load situation on the grid, which is always difficult to estimate or predict.

This leads to a huge challenge of PLC system verification. First of all, an accurate reproduction is impossible due to the complicated time-varying channel conditions, if the devices under test (DUTs) are directly tested in a real power grid. An artificial channel reproduction is therefore required. Next, it is also difficult to reconstruct these channel characteristics accurately with conventional laboratory equipments and simple analog circuits, thus a digital solution is needed. Furthermore,

B. Han, V. Stoica, C. Kaiser, N. Otterbach and K. Dostert are with the Institute of Industrial Information Technology, Karlsruhe Institute of Technology, 76187 Karlsruhe, Germany e-mail: (see http://www.iiit.kit.edu/mitarbeiter.php).

although off-line software implementations of channel simulation can be exploited to flexibly and accurately reconstruct the power line channel behaviors, the latencies of interfacing to the PLC devices can be critical for the performance evaluation. Thus, an real-time hardware setup is essential. Motivated by this, *Götz* proposed an universal solution: to emulate power line channels with a configurable channel emulator, based on a field programmable gate array (FPGA), which was able to emulate usual power line channels flexibly and accurately [3]. Following this idea, different types of power line channel emulators have been developed in the past decade, according to different operation frequency bands of PLC systems. For BB-PLC, *Cañete* et al. proposed an emulator for indoor power line channels in the frequency range up to 30 MHz [8], *Weling* et al. contributed to the multiple-input multiple-output (MIMO) PLC channel emulation [9]–[11]. For NB-PLC, *Liu* introduced a channel emulator with a detailed methodology of PLC system evaluation [12].

Comparing to BB-PLC, NB-PLC has a longer history, and has been more and throughly investigated. As the deployment of long-wave radios has been world-widely vanishing since years, the risk of interfering with radio also keeps sinking in the narrowband field. NB-PLC bands have been licensed widely over the world and some NB-PLC products have been on the market for years. However, due to restricted bandwidth, NB-PLC systems have very constrained data transmission rates (below 500 kbit/s). BB-PLC has been investigated aiming at higher transmission rates up to several hundred Mbit/s, but due to its immaturity in technology and its higher risk of interfering with primary users, its industrial applications are still limited. The selection of a frequency band for a PLC system, therefore, depends always on the application scenario and the local regulations. Traditionally, every PLC system was optimized for an a-priori defined frequency range, which was inflexible. Aiming at applications that are able to work over extended frequency spans with complicated and sundry scenarios, *Liu* et al. developed a new PLC system, which adaptively selects its carrier frequency between 0.15 - 10 MHz [13].

However, no existing literature can fully support complete and flexible channel characterization and emulation in this frequency range yet, especially when focusing on the noise scenario. For example, the mains-synchronous time envelope of narrowband noise is significant in NB-PLC [12], but often ignored in BB-PLC [8]. The random play-back method of *Weling* et al. is appropriate for noise generation in any frequency range [9], but depends on a huge data base and does not

support flexible configuration of noise in a particular category. Furthermore, different types of noise should be extracted from the overall noise for accurate characterization and emulation, but most current noise decomposition techniques are either primitive or dependent on specialized hardware such as orthogonal frequency-division multiplexing (OFDM) systems.

In this article, we propose a systematic approach of LV power line noise characterization and emulation between 0.15 and $10\,\mathrm{MHz}$. A general description of the power line noise and a review of the existing noise models is first given in Section II, followed by the noise characterization in Section III, including the noise decomposition and the noise parameterization. Based on the parametric models, an FPGA-based solution of noise emulation is introduced in Section IV. In Section V, we present a power line noise measuring setup, and show the results of characterization and emulation of a real laboratory measurement as a verification. Finally, Section VI closes our contribution with conclusions and an outlook.

II. LV Power Line Noises: Existing Models

Power line networks are usually divided into three levels: high voltage (HV, 110 - 380 kV), medium voltage (MV, 10 - 30 kV) and low voltage (LV, $\leq$ 0.4 kV) [14]. Due to its wide distribution, easy access and low cost for signal coupling, the LV level attracts the most interest. On this level, research on the noise scenarios focuses mainly on the receiving side, i.e. at power access points such as indoor power outlets and LV transformer stations [2], [4], [15]–[18], but attempts to characterize the noises at their sources have also been reported [19]–[21]. In the recent years, with the arising interest in multi-input multi-output (MIMO) PLC technology, the noise in MIMO PLC channels was also investigated [6], [22]–[24].

A. Noise Classification and the Additive Noise Model

The power line noise at a receiver is hard to characterize with one universal model, because noise origins are found in numerous different sources, and can therefore exhibit quite different behaviors. Hence, *Hooijen* initiated to model the NB power line noise as a summation of four different types, which are classified according to their spectral and time behaviors [25]. This additive model was then extended by *Zimmermann* and *Dostert* to broadband with five updated noise categories: colored background noise (CBGN), narrowband noise (NBN), periodic impulsive noise synchronous to mains (PINS), periodic impulsive noise asynchronous to mains (PINAS) and aperiodic impulsive noise (APIN) [26]:

$$n(t) = n_{\mathrm{CBGN}}(t) + n_{\mathrm{NBN}}(t) + n_{\mathrm{PINS}}(t) + n_{\mathrm{PINAS}}(t) + n_{\mathrm{APIN}}(t). \tag{1}$$

The main sources of these types of noise were also referred to. CBGN originates mainly from summation of numerous noise sources with low power. NBN is mainly caused by broadcast radio signals, which are coupled into the power line network through cables long enough to operate as antennas. *Cortés* et al. added that electrical appliances with a transmitter or a receiver can also cause NBN [4]. PINS and PINAS are generated by power supplies synchronous with the mains cycle

and switching power supplies, respectively. APIN is caused by switching transients in the network, its power spectral density (PSD) can reach more than 50 dB above the CBGN. When measured at an isolated power consumer, it is stated that mainly PINS and PINAS are significant [20].

B. The CBGN Model

To characterize the colored background noise with its scale and spectral power distribution, *Zimmermann* modeled it as a filtered Gaussian white noise (WGN):

$$n_{\mathrm{CBGN}}(t) = \sigma \cdot n_W(t) * h_{\mathrm{CBGN}}(t), \tag{2}$$

where $n_{\mathrm{CBGN}}(t)$ is the CBGN, $n_{\mathrm{W}}(t)$ is a WGN with unity power, σ is the constant standard deviation and $h_{\mathrm{CBGN}}(t)$ is a linear time-invariant (LTI) filter [27]. This model considers the CBGN as a stationary process.

However, the CBGN has been reported in many references to exhibit a periodic PSD [4], [28], [29], and appears cyclostationary. Therefore, two advanced models have been introduced: the temporal cyclostationary model [30] and the spectrotemporal cyclostationary model [31], which can be summarized as

$$n_{\mathrm{CBGN,T}}(t) = \sigma(t) \cdot n_{\mathrm{W}}(t) * h_{\mathrm{CBGN}}(t) \tag{3}$$

$$\text{and } n_{\mathrm{CBGN,ST}}(t) = n_{\mathrm{W}}(t) * h_{\mathrm{CBGN}}(t, \tau), \tag{4}$$

respectively. Here, $\sigma(t)$ is a time-varying deviation and $h_{\mathrm{CBGN}}(t, \tau)$ is a linear periodic time varying (LPTV) filter which fulfills

$$h_{\mathrm{CBGN}}(t, \tau) = h_{\mathrm{CBGN}}(t, \tau - nT_0) \qquad \forall n \in \mathbb{Z}, \tag{5}$$

where T_0 is the cyclic period, normally equal to one half of the mains period. Comparing the two models, it can be asserted that the temporal cyclostationary model is also a special case of the general spectrotemporal cyclostationary model, where only the scale but not the shape of the noise PSD varies over time.

Taking the spectrotemporal cyclostationary model, the characterization of the CBGN equals to the characterization of the LPTV filter $h_{\mathrm{CBGN}}(t, \tau)$, which can be expressed as a Volterra series [12]:

$$h_{\mathrm{CBGN}}(t, \tau) = h_1(\tau) + \sum_{n=2}^{+\infty} \int \int \cdots \int h_n[t, \tau_1, \ldots, \tau_{n-1}] \cdot \prod_{i=1}^{n-1} m(t - \tau_i) \mathrm{d}\tau_1 \mathrm{d}\tau_2 \ldots \mathrm{d}\tau_{n-1}, \tag{6}$$

where $h_n(t_1, t_2, \ldots, t_n)$ is the nth Volterra kernel and $m(t)$ is a periodic function of time. However, not only the estimations of the kernels and $m(t)$, but also synthetic implementation of this model can be computationally complex. Therefore, in practice, it is more appropriate to assume that $h_{\mathrm{CBGN}}(t, \tau)$ is underspread for power line channels, i.e. its coherence time is larger than its effective impulse response [8]. Under this assumption, the LPTV filter $h_{\mathrm{CBGN}}(t, \tau)$ can be approximated

with a linear switching time-varying (LSTV) filter:

$$h_{\text{CBGN}}(t,\tau) = \begin{cases} h_1(t), & \tau \in [nT_0, \tau_1 + nT_0) \\ h_2(t), & \tau \in [\tau_1 + nT_0, \tau_2 + nT_0) \\ \dots \\ h_K(t), & \tau \in [\tau_{K-1} + nT_0, T_0 + nT_0) \end{cases}$$
$$\forall n \in \mathbb{Z}, \quad (7)$$

where the system switches among K different LTI filters sequentially in every period. By modifying K, the time resolution of the characterization can be configured. The LSTV approximation for LPTV systems was mathematically derived by *Mehr* et al. [32] and has been demonstrated as efficient in research on power line channels [8], [33]. Thus, the characterization of the CBGN is further simplified into the characterizations of K LTI filters and the estimations of K switching times. Hence, we take the LSTV model in our work for CBGN.

C. The NBN Model

The NBN can be generally modeled as a summation of different independent harmonic interferences, as proposed in [26]:

$$n_{\text{NBN}}(t) = \sum_{i=1}^{N_{\text{NBN}}} c_{\text{NBN},i}(t) = \sum_{i=1}^{N_{\text{NBN}}} A_i(t) \sin(2\pi f_i t + \phi_i(t)),$$
$$(8)$$

where N_{NBN} is the number of independent interferences, $A_i(t)$, f_i and $\phi_i(t)$ are the time envelope, the central frequency and the phase of the ith interference $c_{\text{NBN},i}(t)$, respectively. Self-evidently, each $c_{\text{NBN},i}$ can also be expressed as

$$c_{\text{NBN},i}(t) = A_i(t) \sin(2\pi (f_i + \Delta f_i(t))t), \quad (9)$$

where $f_i + \Delta f_i$ is an instantaneous frequency. The frequency offset Δf_i is normally random and always within a certain bandwidth B_i:

$$|\Delta f_i| < \frac{B_i}{2}. \quad (10)$$

The bandwidths of NBNs in narrowband have been statistically analyzed by *Bausch* et al., reporting an average value of about $3\,\text{kHz}$ [34]. For the NBNs at higher frequencies, the bandwidths can reach up to some ten kHz [7]. In this paper, the model (9) is taken for NBN.

Investigating the statistical behavior of NBN deeper, both *Cortés* [4] and *Opalko* [35] pointed out that there are two different classes of some narrowband interferences. The first class is stationary NBN, for which the auto-covariance is time-invariant, i.e.

$$C_{c_{\text{NBN},i} c_{\text{NBN},i}}(t_1, t_1 + \Delta t) = C_{c_{\text{NBN},i} c_{\text{NBN},i}}(t_2, t_2 + \Delta t)$$
$$\forall t_1, t_2, \Delta t \in \mathbb{R}. \quad (11)$$

The second class is cyclostationary NBN, whose auto-covariance is periodic:

$$C_{c_{\text{NBN},i} c_{\text{NBN},i}}(t, t + \Delta t)$$
$$= C_{c_{\text{NBN},i} c_{\text{NBN},i}}(t + nT_{\text{NBN}}, t + nT_{\text{NBN}} + \Delta t) \quad (12)$$
$$\forall i \in \{1, 2, \dots N\}, \quad \forall n \in \mathbb{Z}, \quad \forall t, \Delta t \in \mathbb{R},$$

where T_{NBN} is the cyclic period. Noticing that (11) also fulfills (12), it can be asserted that the latter one is the general case.

More accurately, *Cortés* et al. pointed it out in [4] that cyclostationary NBN is synchronous with the mains. We have verified this assertion in previous research work by showing that T_{NBN} equals one half of the mains period for this kind of NBN [36]. The source of the cyclostationarity, according to *Liu*, is the periodic terms in the envelopes $A_i(t)$, which are synchronous to the mains period [12]. Although the amplitude of a narrowband interference is not totally deterministic but still stochastic to a certain degree, the random fluctuation is usually neglected and the envelope is approximately assumed to be either constant (for stationary NBN) or a periodic function synchronous to the mains (for cyclostationary NBN).

Considering the periodicity of a narrowband interference $\sin(2\pi (f_i + \Delta f_i(t))t)$ and its envelope $A_i(t)$, their product will include a set of harmonics. Thus, according to [36] the model (9) can also be transformed into another form:

$$n_{\text{NBN}}(t) = \sum_{i=1}^{N_{\text{NBN}}} A_i e^{j\Delta\phi_i} \sum_{l=1}^{L} c_{i,l} e^{j2\pi f_{i,l} t}, \quad (13)$$

where L is the number of harmonics in each independent interference, A_i and $\Delta\phi_i$ are the constant scaling factor and the phase-offset of the ith interference. $c_{i,l}$ and $f_{i,l}$ are the coefficient and the central frequency of the lth harmonic in the ith interference, respectively. However, due to the flexibility of using bandwidth instead of phase in the characterization, we still take the form (9) in this paper as the NBN model.

D. The Periodic Impulsive Noise Model

PINS and PINAS, despite their different sources and cyclic periods, have no substantive distinction in their time behavioral patterns. Therefore, they are also usually collectively referred to as the periodical impulsive noise (PIN). Similar to the NBN, the PIN at receiver is also considered as a summation of different independent PIN components:

$$n_{\text{PIN}} = \sum_{i=1}^{N_{\text{PIN}}} c_{\text{PIN},i}(t), \quad (14)$$

where N_{PIN} is the amount of components. For each component $c_{\text{PIN},i}$, the amplitude probability distibution, according to *Katayama* et al., matches a Gaussian model [30]. Based on these facts, *Ohne* and *Katayama* proposed the well-known cyclostationary Gaussian model [30], [37]–[39], describing the cyclostationary component in a power line noise as a Gaussian noise with the time-varying power:

$$\sigma_{\text{PIN},i}^2(t, f) = \sigma_{\text{PIN},i}^2(t) a_i(f), \quad (15)$$

where $\sigma_{\text{PIN},i}^2(t)$ is a periodical function, and $a_i(f)$ describes the frequency dependency.

It has been reported in different works that the PSD of PIN is significantly higher than the background noise in a wide frequency range up to $100\,\text{MHz}$ [4], [17]. This leads to less importance of the frequency dependency $a_i(f)$ of a PIN component, but a higher interest in $\sigma_{\text{PIN},i}^2(t)$. To describe this time behavior and to identify PIN components, three
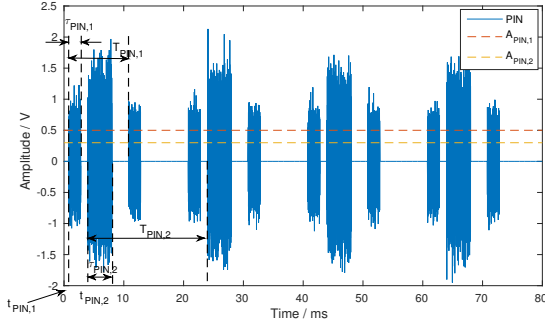
Figure 1: A PIN with two independent components.

parameters have been generally applied since long: the impulse amplitude, the impulse width and the interarrival time between impulses [14], [26]. In practice, it is often necessary to approximate the periodical fluctuation of the PIN power with on-off-keying [12], [40]. An example with two PIN components is illustrated in Fig. 1, where $A_{\text{PIN},i}$, $t_{\text{PIN},i}$, $\tau_{\text{PIN},i}$ and $T_{\text{PIN},i}$ are the impulse amplitude, the arriving time, the impulse width and the interarrival time of the component $c_{\text{PIN},i}$, respectively. There is

$$\sigma^2_{\text{PIN},i}(t) =$$
$$\begin{cases} A_{\text{PIN},i} & : t \in [t_{\text{PIN},i} + nT_{\text{PIN},i}, t_{\text{PIN},i} + \tau_{\text{PIN},i} + nT_{\text{PIN},i}]; \\ 0 & : \text{otherwise}, \end{cases}$$
$$(16)$$

$$\forall n \in \mathbb{Z};$$

This is equivalent to the spectrotemporal cyclostationary model (4), which was applied on PIN by *Lin* et al. in [41]:

$$c_{\text{PIN},i} = n_{\text{W}}(t) \otimes h_{\text{PIN},i}(t), \qquad (17)$$
$$h_{\text{PIN},i}(t, \tau) =$$
$$\begin{cases} A_{\text{PIN},i}\delta(t) & : \tau \in [t_{\text{PIN},i} + nT_{\text{PIN},i}, t_{\text{PIN},i} + \tau_{\text{PIN},i} + nT_{\text{PIN},i}]; \\ 0 & : \text{otherwise}, \end{cases}$$
$$(18)$$

$$\forall n \in \mathbb{Z}$$

There are also other PIN models available, such as the autoregressive moving-average (ARMA) model proposed by *Gianaroli* et al. in [18]. Nevertheless, in comparison, the spectrotemporal cyclostationary model (17) has only four parameters, which are easy to obtain from measurements, and is hence taken for PIN in our work.

E. The APIN Model

Due to the nature of its source, APIN exhibits no deterministic behavior. It is a common way to describe it with the Middleton's Class-A model [42]–[45]:

$$p(n_A) = \sum_{m=0}^{\infty} P_m \frac{1}{\sqrt{2\pi\sigma^2_m}} exp(-\frac{n^2}{2\sigma^2_m}), \qquad (19)$$

$$P_m = \frac{e^{-A}A^m}{m!}, \qquad (20)$$

$$\sigma^2_m = \sigma^2 \frac{m/A + \Gamma}{1 + \Gamma} = \sigma^2_i \frac{m}{A} + \sigma^2_g, \qquad (21)$$

$$\Gamma = \frac{\sigma^2_g}{\sigma^2_i}, \qquad (22)$$

where $p(n_A)$ is the probability density function (PDF) of the noise amplitude. A is the so-called impulsive index, i.e. the noise becomes more impulsive when A is small and more Gaussian when it is large. σ^2, σ^2_g and σ^2_i are the powers of the overall noise, the Gaussian noise and the impulsive noise, respectively.

Another common approach of APIN is to separately describe the occurrence and the amplitude, which can be included in a time-discrete form as

$$n_{\text{APIN}}[k] = \Phi[k]n_{\text{G}}[k], \qquad (23)$$

where n_{G} is a white or colored Gaussian noise and Φ is a random process that denotes the presence of APIN when it takes on the value of 1, and the absence of APIN when it is 0. One well-known model of this kind is the Bernoulli-Gaussian model [46], [47], where Φ is a Bernoulli process. Another widely used model of this kind is the partitioned Markov chain model proposed by *Zimmermann* et al. in [26]. Defining $N_D + N_W$ states, a Markov chain is shown in Fig. 2, where N_D states are grouped in a set $\mathbf{A}$ and N_W in another set $\mathbf{B}$. At the time $t = kT_s$, where T_s is the sampling interval, the Markov chain gives the output function:

$$\Phi[k] = \begin{cases} 0, & z[k] \in \mathbf{A} \\ 1, & z[k] \in \mathbf{B} \end{cases}. \qquad (24)$$

The probability of transitions between states can be summarized with the matrix in (25), where

$$u_{i,t_1} = 1 - u_{i,i}, \qquad (26)$$
$$g_{i,t_2} = 1 - g_{i,i}. \qquad (27)$$

This matrix can be estimated according to the measured statistics of APIN's pulse width and interarrival time [26], which are defined similarly as for PIN in Fig. 1. Introducing the statistical knowledge of amplitude into the present model (24), the APIN can be modeled in the discrete-time domain as

$$n_{\text{APIN}}[k] = n_{\text{APIN}}(kT_s) = A_{\text{APIN}}\Phi[k] \cdot n_{\text{G}}(kT_s), \qquad (28)$$

where A_{APIN} is the amplitude.

Compared to the Middleton's Class-A model and the Bernoulli-Gaussian model, the partitioned Markov chain model is more accurate, more flexible, benefits from separating the APIN from the CBGN and quantitatively modeling the impulse width. Hence it is taken in our work for APIN.
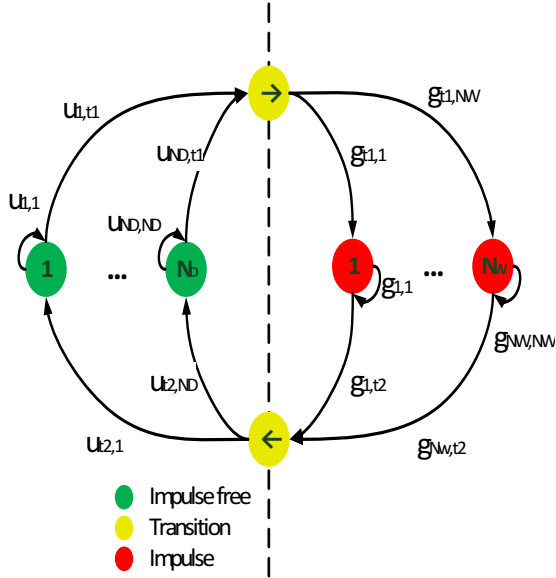
Figure 2: Partitioned Markov chain to represent the APIN events, where the two transition states have no physical meaning but are intended to simplify the mathematical model. $u_{i,j}$ and $g_{i,j}$ represent the probabilities of transition between two states [26].

III. DECOMPOSITION AND PARAMETERIZATION

So far, existing power line noise models are reviewed and for each type of PLC noise we have selected a model, which has been validated in literature. Based on these models, a parametric characterization of power line noise scenarios can be realized. For a better characterizing accuracy, different types of noise should be first decomposed from the mixed measurement, before the parameter estimation is executed. However, till now, most existing work about PLC noise scenarios only applies analytic techniques on raw measurements and manually evaluates the results [4], [6], [26], [44]. A variety of noise cancellation methods have been developed for robust PLC systems [41], [45], [48], but they aim at recovering the transmitted symbols with specific modulation schemes and transmission methods, and cannot be used for noise decomposition. *Liu* proposed several synthetic extraction methods for different noise types to support his NB-PLC channel emulation [12], but yet primitive. In this section, we collectively present a complete set of methods to decompose a mixed PLC noise into its components. All these methods work entirely on the physical layer, depending on no modulation scheme, transmission method or coding and require no specialized hardware, either. Afterwards, for each type of noise, we also give the key model parameters as well as their estimates.

A. Extraction and Parameterization of CBGN

The CBGN, due to its relatively low power and variant behavior, is hard to be extracted first. But it can be obtained from the residual after the extractions of other types of noise. Therefore, here we focus on the parameterization of CBGN.

Taking the LSTV model 7, the CBGN can be described by the following parameters:

1) the number of LTI filters (states) K,
2) $K-1$ switching times $\tau_1, \ldots, \tau_{K-1}$,
3) K sets of coefficients $\mathbf{H}_1, \ldots, \mathbf{H}_K$, which are the discrete frequency responses of the LTI filters $h_1(t), \ldots, h_K(t)$.

For convenience, we set the number of LTI filters fixed as $\hat{K} = 10$ and equally divided each cyclic (mains) period so that $\hat{\tau}_i = \frac{iT_0}{K}$. When the model is in its ith state, i.e. $h_{\text{CBGN}}(t, \tau) = h_i(t)$, according to (4) there is

$$N_{\text{CBGN}}(f) = N_{\text{W}}(f)H_{\text{CBGN}}(f, t) = N_{\text{W}}(f)H_i(f) \quad (29)$$

Remembering that n_{W} is of unity power, there is

$$|H_i(f)| = \sqrt{\frac{S_{\text{CBGN}}(f)}{S_{\text{W}}(f)}} = \sqrt{S_{\text{CBGN}}(f)}, \quad (30)$$

where $S_{\text{CBGN}}(f)$ and $S_{\text{W}}(f)$ are the PSD of n_{CBGN} and n_{W}, respectively.

Hence, given an extracted CBGN which lasts M mains periods, the fragment in each mains period can be further evenly segmented into 10 frames, and the frequency response of the ith LTI filter is estimated as

$$\hat{H}_i[n] = \frac{1}{M}\sum_{j=1}^{M}\hat{N}_{\text{CBGN},i,j}[n], \quad (31)$$

where M is the number of mains periods in the measurement and $\hat{N}_{\text{CBGN},i,j}$ is the DFT of the ith CBGN frame in the jth mains period.

B. Extraction and Parameterization of NBN

Different from the situation in wireless communication, narrowband interferences in PLC are sometimes challenging to detect due to their time-dependent envelopes, which reduce the efficiency and accuracy of simple time-invariant spectral peak detection. In a previous work of ours [36], we already proposed a method to extract the periodic NBN components from raw noise measurements. This so-called narrowband regression (NBR) method showed a good performance in verifications through real measurement tests and simulations. To obtain the NBNs from the raw noise measurement, here we also adopt the NBR method, which can be briefly summarized as follows.

1) A frequency mask of 11 pins spacing from each other by $100\,\text{Hz}$ is shifted along the spectrum of the measured noise, to detect the strongest narrowband interference and its harmonics generated by the mains period modulation (the envelope).
2) A recursive least-square (RLS) estimator based on the model (13) is used to estimate the detected NBN and its harmonics.
3) The estimation is removed from the noise and the residual is sent back to the detector in step 1 to find the next independent narrowband interference. The algorithm runs iteratively until it converges or no more NBN can be detected.

$$\mathbf{P} = \begin{bmatrix} u_{1,1} & \cdots & 0 & u_{1,t_1} \cdot g_{t_1,1} & \cdots & u_{1,t_1} \cdot g_{t_1,N_W} \\ \vdots & \ddots & \vdots & \vdots & \ddots & \vdots \\ 0 & \cdots & u_{N_D,N_D} & u_{N_D,t_1} \cdot g_{t_1,1} & \cdots & u_{N_D,t_1} \cdot g_{t_1,N_W} \\ g_{1,t_2} \cdot g_{1,t_2} & \cdots & g_{1,t_2} \cdot u_{t_2,N_D} & g_{1,1} & \cdots & 0 \\ \vdots & \ddots & \vdots & \vdots & \ddots & \vdots \\ g_{N_W,t_2} \cdot u_{t_2,1} & \cdots & g_{N_W,t_2} \cdot u_{t_2,N_D} & 0 & \cdots & g_{N_W,N_W} \end{bmatrix}, \tag{25}$$

Table I: Test result of NBN central frequency estimation, in kHz

	f_1	f_2	f_3	f_4
Simulation model	302.00	470.00	54.00	84.00
Estimation	301.50	470.00	54.50	83.50

(a) Constant envelope for the NBNs 1 and 2.

(b) Periodic envelope for the NBNs 3 and 4.

Figure 3: The NBN envelopes estimated from the synthesized test noise.

Detailed algorithm and implementation of the NBR method are available in [36].

The NBR method extracts every independent interference separately from the measurement, so that the parameterization can easily follow. According to the model (9), each independent interference $c_{\mathrm{NBN},i}(t)$ can be characterized by the following parameters:

1) the central frequency f_i,
2) the bandwidth B_i,
3) the periodical envelope $A_i(t)$.

Here, f_i and $A_i(t)$ are already estimated through the execution of the NBR method, while the B_i can be obtained either through further spectral analysis of the extracted signal, or from the a-priori knowledge of existing radio sources at its corresponding central frequency f_i, if available.

As an example we verified our method with a synthesized noise, which includes a WGN and 4 independent narrowband interferences with different carrier frequencies. Each interference is amplitude-modulated with a WGN and has $9\,\mathrm{kHz}$ bandwidth as normal AM radio signals. Two interferences have constant time envelopes and the other two are further modulated with a $100\,\mathrm{Hz}$ triangle envelope. The results are shown in Table I and Fig. 3

C. Extraction and Parameterization of PIN

Also in [36] we introduced a so-called multiple cyclic regression (MCR) method to extract PINs with known cyclic frequencies. This method, as described in its original source [49], is an adaptive LSTV filter array which minimizes the least square estimation error, and hence fits the LSTV-based PIN model (4,16) well. Here we simply exploited the same approach to detect and extract all PINs from the nosie residual after the NBN extraction. The procedure can be briefly summarized as follows.

1) Calculate the cyclic coherence function (CCF) $C_{N_rN_r}(f,\alpha)$ [50] of the noise measurement $n_r = n - n_{\mathrm{NBN}}$, from which the NBN component has been removed. Integrate $C_{N_rN_r}(f,\alpha)$ over f. Peaks can be observed at the existing cyclic frequencies $\alpha_1, \ldots, \alpha_{N_{\mathrm{Cyclic}}}$ and their harmonics.
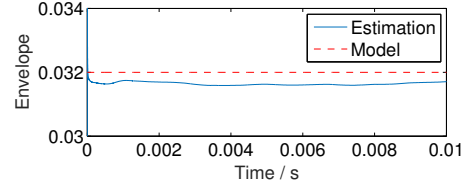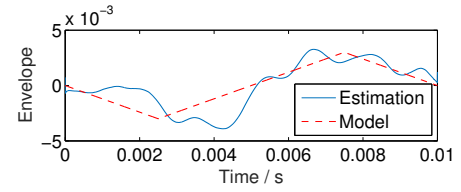
2) For each detected cyclic frequency α_i, the MCR method is called to cancel the corresponding cyclic component $\hat{n}_{\alpha_i}$.

Detailed algorithm and implementation of the MCR method can be found in [36].

Taking the model (16), to characterize a PIN component $c_{\mathrm{PIN},i}$, the impulse amplitude $A_{\mathrm{PIN},i}$, the impulse width $\tau_{\mathrm{PIN},i}$ and the interarrival time $T_{\mathrm{PIN},i}$ are necessary. Especially, for a PIN synchronous to the mains voltage, its relative time offset $t_{\mathrm{PIN},i}$ to the mains period is also of interest, because the performance of PLC devices can be synchronous to the mains voltage [51]. It should be noticed here that the number of cyclic frequencies detected in the extraction process N_{Cyclic} is not the number of independent PIN components N_{PIN}, because several PIN components can have the same cyclic frequency. Therefore, for each extracted cyclic component $\hat{n}_{\alpha_i}$ first we applied a variance-based thresholding on every PIN we extracted to obtain a binary envelope:

$$e_{\alpha_i}(t) = \begin{cases} 1 & \hat{n}_{\alpha_i}(t) > 5\hat{\sigma}_{\alpha_i} \\ 0 & \text{otherwise,} \end{cases} \tag{32}$$

where $\hat{\sigma}_{\alpha_i}$ is the median variance of $\hat{n}_{\alpha_i}$. If multiple pulses are observed in e_{α_i} during one cyclic period, which means more than one PIN sources of the same cyclic frequency α_i are present, the envelope $e_\alpha(t)$ must be further decomposed:

$$e_{\alpha_i}(t) = \sum_{k=1}^{N_{\alpha_i}} e_{\alpha_i,k}(t), \tag{33}$$

where N_{α_i} is the number of continuous pulses per cyclic period in e_{α_i}, and each $e_{\alpha_i,k}$ contains an individual pulse, which corresponds to an independent PIN component. From $e_{\alpha_i,k}$, the PIN's interarrival time T_{PIN} can be computed as $\frac{1}{\alpha_i}$, and the pulse width τ_{PIN} can be simply measured. Furthermore, if the measurement is synchronized to the mains period, t_{PIN} can also be obtained. Then we estimate the amplitude of each PIN according to the power:

$$\hat{A}_{\alpha_i,k} = \frac{\int (\hat{n}_{\mathrm{W}}(t) e_{\alpha,i}(t))^2 \mathrm{d}t}{\int \hat{n}_{\mathrm{PIN}}^2(t) \mathrm{d}t}, \tag{34}$$

where $\hat{A}_{\alpha_i,k}$ is the estimated amplitude of the kth PIN with cyclic frequency α_i, and $n_{\mathrm{W}}(t)$ is a zero-meaned WGN with unity variance.

An example test was executed with a synthesized noise, which included a background WGN and two PINs synchronous to the mains period. Both PINs were synthesized with WGN and a periodic rectangular time window. The result is shown in Table II.

D. Extraction and Parameterization of APIN

Comparing to the cyclostationary CBGN, APIN exhibits a extremely high instant power and a strong non-stationarity. The APIN extraction, therefore, is mathematically similar to the artifact removal in some biomedical signal processing subjects, where artificial peaks are also short in duration, high in amplitude, with strong non-stationarity and usually caused by transitions in the system such as plugging and unplugging devices [52], [53]. So we modified the robust artifact removal algorithm proposed in [54] to decompose the APIN.

The modified approach is implemented based on a robust APIN detection method and a robust noise reconstruction method, as shown in Fig. 4. First, the residual of the raw measurement $n(t)$ after removing the NBN $\hat{n}_{\mathrm{NBN}}(t)$ and the PIN $\hat{n}_{\mathrm{PIN}}(t)$ is sent to the APIN detector for a brief examination. If no APIN is detected, the process will be terminated. Otherwise, a short segment with one detected impulse will be extracted from the input to reduce the amount of computation, and this segment is then reconstructed to cancel the APIN. After replacing the detected impulse with the reconstructed noise, the result is sent back to the detector to search for the next aperiodic impulse. This process keeps recursing until no more APIN can be detected, so that an APIN-free residual as well as an extracted APIN can be obtained.

The APIN detector is implemented with a deviation-based thresholding:

$$D_x[n] = \begin{cases} 1 & |x[n]| \geq \beta \sigma_x \\ 0 & \text{otherwise}, \end{cases} \tag{35}$$

where β is a significance factor implying the level of APIN compared to the rest part of noise. σ_x is the deviation of x, $D_x[n]$ takes on the value of 1 when the noise sample $x[n]$ is contaminated by an APIN, and 0 when $x[n]$ is APIN-free. Considering that the strength of APIN may influence the normal standard deviation of x, for a robustness we computed the median absolute deviation:

$$\sigma_x = \text{median}_i(|x[i] - \text{median}_j(x[j])|) \tag{36}$$
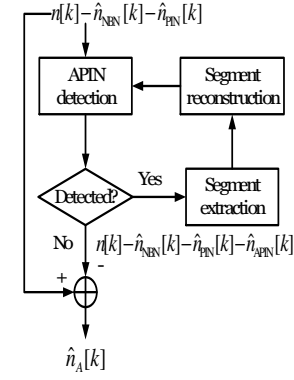
Figure 4: The proposed APIN extraction method in discrete time domain. $n[k]$, $\hat{n}_{\mathrm{NBN}}[k]$, $\hat{n}_{\mathrm{PIN}}[k]$ and $\hat{n}_{\mathrm{APIN}}[k]$ are the raw measurement, the extracted NBN, the extracted PIN and the extracted APIN, respectively.
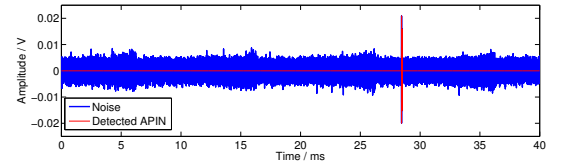
(a) Overview
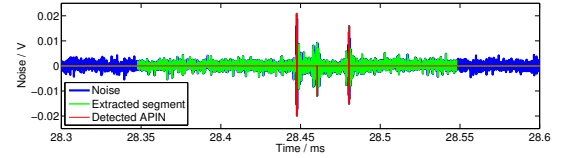
(b) Zoom-in. Note that the segment was selected based on the first detected APIN sample, but also covered several other APIN samples.

Figure 5: An example of APIN detection and segment extraction.

Due to the fact that the APIN peaks are significantly high, we set $\beta = 10$. According to [26], only 1% among all impulses in PLC last longer than $200\,\mu\text{s}$, so we extracted a $200\,\mu\text{s}$ segment around the strongest detected impulse sample. An example of the APIN detection and the segment extraction is shown in Fig. 5. As the next step, to separate the APIN from the CBGN, we made use of its high non-stationarity. First we deployed the empirical mode decomposition (EMD) on the extracted segment with aperiodic impulse. The EMD, known as part of the Hilbert-Huang-Transform (HHT), decomposes a signal into a finite set of nearly orthogonal components, which are described as the signal's intrinsic mode functions (IMFs). Comparing to other analyzing techniques such as the short-time Fourier-Transform (STFT) or the wavelet transform, it does not leave the time domain, depends on no base-wave selection, and is thus highly adaptive and effective. Further information about this algorithm can be found in its original source [55]. Applying the EMD to an extracted segment $y[k]$,

Table II: Test result of PIN estimation

	T_{PIN} (ms)		τ_{PIN} (µs)		t_{PIN} (µs)		A_{PIN}	
	Estimation	Ground truth	Estimation	Ground truth	Estimation	Ground truth	Estimation	Ground truth
$c_{PIN,1}$	10	10	93.1	100	1026	1000	1	0.97
$c_{PIN,2}$	10	10	221.5	230	3013	3000	0.5	0.42

we got its IMF set $M_y^i[k], i \in \{1, \ldots, N\}$, where

$$\sum_{i=1}^{N} c_i^y[k] = y[k]. \qquad (37)$$

An example is shown in Fig. 6.

Differing from the original method proposed in [54] for biomedical signals, here we modeled every IMF as an autoregressive moving average (ARMA) process instead of an autoregressive integrated moving average (ARIMA) process, because a power line noise does not include any long-term trend, which cannot be presented by ARMA models but only by ARIMA models. For each ith IMF we estimated its model order (p_i, q_i) with the estimator introduced by *Box* et al. [56]:

$$\hat{p}_i = \arg \min_{k \in \mathbb{N}} (R_i[k] < 0.05) - 1, \qquad (38)$$

$$\hat{q}_i = \arg \min_{k \in \mathbb{N}} (P_i[k] < 0.05) - 1, \qquad (39)$$

where $R_i[k]$ and $P_i[k]$ are the autocorrelation function (ACF) and partial autocorrelation function (PACF) of $c_i^y[k]$. If $\hat{p}_i \leq 20$, we used the robust filter cleaner introduced by *Zoubir* et al. [57] to rebuild it as under the ARMA$(\hat{p}_i, \hat{q}_i)$ model, so that a "cleaned" reconstruction $\hat{c}_i^y[k]$ is obtained. Otherwise, the IMF may turn out as too high-ordered and contains only low-frequency components, which are almost independent of broadband impulses. In this case we directly used the original IMF for the reconstruction, i.e. $\hat{c}_i^y[k] = c_i^y[k]$. Summing all reconstructed IMFs, we managed to reconstruct the extracted segment, as shown in Fig. 6. Removing the reconstruction from the extracted segment, the APIN component can be obtained.

According to *Zimmermann* [26], statistics of the pulse amplitude A_{APIN}, the pulse width τ_{APIN}, the pulse distance Δt_{APIN} and the arriving time t_{APIN} are needed for APIN characterization. *Liu* has presented a transform from these statistics to the parameters of the Markov-chain model shown in Fig. 2 [12]. Hence we can record the amplitude, the pulse width and the arriving time of every single extracted impulse, so that the essential statistics can be obtained from a large-sized measurement which lasts several hours or even days.

IV. EMULATION

As *Götz* [3], *Liu* [12] and *Cañete* [8] showed, based on the estimated parameters, the noises of different classes can be generated with an FPGA-based emulator independently, and then summed up for a mixed noise. Here we also adopted this idea and implemented an FPGA-based noise emulator with the structure illustrated in Fig. 7.

According to the estimated central frequencies and bandwidths, direct digital synthesizers (DDSs) generate narrowband interferences based on a look-up table (LUT). The key
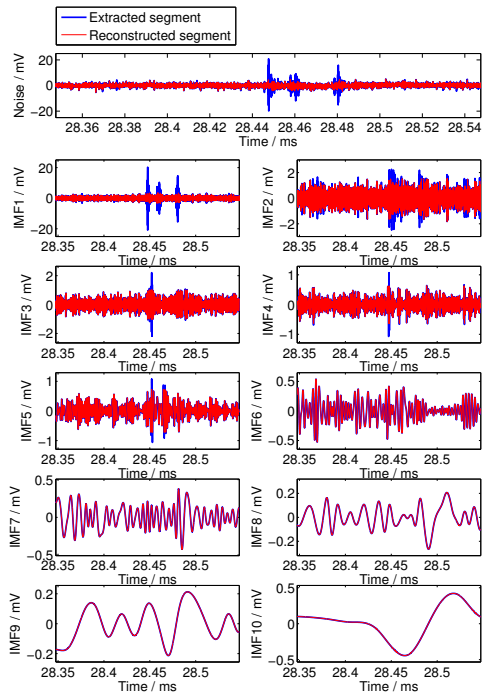
Figure 6: An extracted noise segment with APIN, the reconstructed segment without APIN and their IMFs. The lower a IMF's order is, the higher frequencies it contains. From the 6th IMF on, no ARMA estimation but the original IMF was used for the reconstruction.
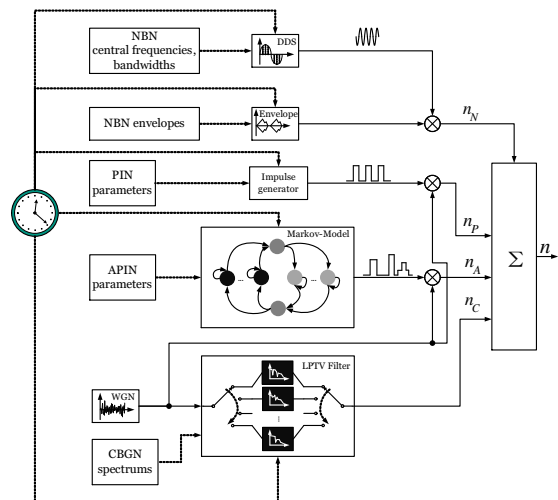
Figure 7: The block diagram of our FPGA-based noise emulation.

idea of this implementation is to sample a sinusoidal curve over one period and store the samples into a LUT. Reading the values in the LUT with a certain clock speed, a single-frequency signal can be synthesized. By modifying the clock speed over time continuously, the frequency will shift over a certain range so that a narrowband signal can be synthesized. Further details can be found in [40]. These synthesized narrowband interferers are then multiplied with their mains-synchronous envelopes, which are stored in the FPGA, so that the NBNs are emulated with time variance. We implemented 12 independent DDSs so that up to 12 different NBNs can be emulated at the same time. The LUT is 12 bits wide and 4000 words deep, containing a sinusoidal waveform. Being read by a $200\,\mathrm{MHz}$ clock, it supports generating central frequencies up to $75\,\mathrm{MHz}$ with frequency resolution of $0.5\,\mathrm{kHz}$. The bandwidth can be configured from $0\,\mathrm{Hz}$ to twice the central frequency. Each envelope is quantized with 12 bits and stored in a 1024-word memory block so that a time resolution of about $0.02\,\mathrm{ms}$ is achieved.

Making use of the estimated amplitudes, impulse widths and interarrival times, impulse generators are deployed to generate periodic rectangular impulse series, either synchronous or asynchronous with the mains. These impulse series are then multiplied with synthesized WGN to emulate the PINs. The implementation is able to generate up to 4 independent PINs, supporting repetition periods between $1\,\mu\mathrm{s}$ and $20\,\mathrm{ms}$, impulse widths between $1\,\mu\mathrm{s}$ and $1\,\mathrm{ms}$. The amplitude quantization is 12 bits.

A state-machine module is implemented for the Markov chain APIN model shown in Fig. 2. This module generates aperiodic rectangular impulses according to the estimated APIN statistics. The generated impulses are then multiplied with synthesized WGN and subsequently quantized with 12 bits to emulate the APIN.

To generate the cyclostationary CBGN, up to 10 different LTI filters can be configured with the estimated CBGN spectrum. Switching among these filters cyclically, a LPTV filter is realized. The synthesized WGN is filtered with this LPTV filter. The magnitude is quantized with 12 bits, the frequency resolution is $2.44\,\mathrm{kHz}$. Although we divided each mains period equally into 10 frames in the estimation, the emulator allows flexible timing of switching between LTI filters, with a time resolution of $500\,\mu\mathrm{s}$.

The NBNs, the PINSs and the CBGN are all synchronous with the mains voltage. Depending on the region, an ideal mains voltage is a 50 or 60 Hz sinusoidal wave. However, influenced by the network's load scenario, a real mains voltage always exhibits minor variation of frequency. With help of a zero-crossing detector (ZCD) connected to the grid, we synthesized a global timing signal in the emulator to synchronize the aforementioned noise types. Summing all types of noise up, we could obtain the mixed noise, which is then converted from digital to analog by a DAC and then amplified for final output.

V. MEASUREMENT

As we have introduced before, depending on the interest of research, either the overall channel noise or the power consumer noise can be characterized. Generally, three challenges are to be overcome in the noise measurement at power lines: protecting the devices from the mains voltage and transition peaks; obtaining the synchronization between the noise and the mains phase; isolating the channel/consumer under measurement from the interference generated by the measuring devices. Particularly, when measuring a single power consumer, an additional task of isolating it from the network while supplying it with a "clean" mains voltage must be accomplished as well.

A. Measuring Setup

The problem of device protection can be solved with a LV power line coupler, which behaves as a band-pass filter and isolates the devices from the low-frequency mains voltage. A suppressor-diode-based protection circuitry after it is also needed [14]. In our framework, we used a pre-amplifier instead of a traditional passive diode network as the protecting stage for higher flexibilities with respect to frequency and gain. A zero-crossing detector (ZCD) was also implemented to simplify the acquisition of the mains voltage's phase. An universal software radio peripheral (USRP) was used to capture the coupled noise and the output of the ZCD. Detailed hardware parameters are listed in Table III.

The interference generated by the measuring devices can be avoided in the measurement, if the devices are supplied by a power outlet far away from the measuring point (e.g. at another network phase) and through a mains filter, which is also known as line impedance stabilization network (LISN) [7]. A LISN is a carefully designed symmetric passive low-pass filter, which strongly attenuates all signal and noise portions in the PLC band of interest and passes the mains voltage, as shown in Fig. 8. The same method can also be used to obtain the clean mains voltage for power consumer measurements. According to *Liu*, the performance can be even further improved with an uninterruptible power supply (UPS) instead of the grid as the power source [12].

Based on these hardware devices, we set up our noise measuring equipment as illustrated in Fig. 9. The receiver Rx is supplied by a power outlet on a different network phase through a LISN, so that its own interference will not significantly influence the channel/consumer under test. The power consumer under test is supplied by a UPS over a LISN, so that only its own generated noise will be measured at point B, without interference from the grid. Both the noise and the output of the zero-crossing detector are recorded.

B. Laboratory Measurements

As case studies, we performed three different laboratory measurements: the channel noise at an ordinary power outlet in our office, the noise generated by a dimmer lamp and the noise generated by a monitor. The time waveforms and spectrograms are shown in Fig. 10. It can be observed that the CBGN was insignificant in both consumer noise measurements. Comparing to the dimmer lamp, which showed almost only strong periodic impulses in its noise, the monitor also generated considerable

Table III: Key parameters of the measuring hardware

Analog-to-digital converter	Sampling rate	Input range	Resolution	Input impedance
	25 MSPS	±1.25 V	14 bits	50 Ω
Coupling circuit	Amplifier gain*	Flatness in 10 MHz	**Zero-crossing detector**	Detection pulse width
	0 dB or −20 dB	≤0.5 dB		500 µs
*: An 20 dB attenuation is activated when capturing noise with APIN to prevent the high peaks from clipping. It is deactivated when measuring power consumers which generate no APIN.				
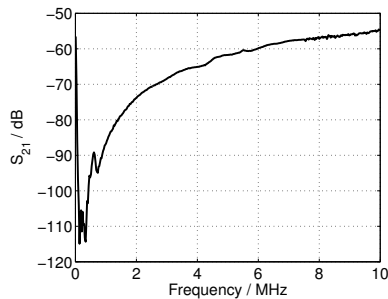
(a) The S_{21} parameter measured with a vector network analyzer (VNA). Strong attenuation can be observed in the entire frequency range of interest.
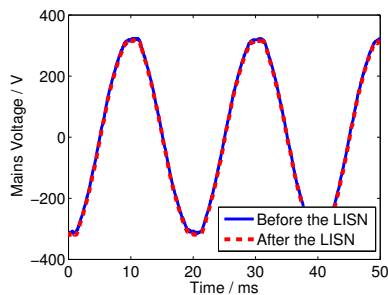
(b) A mains voltage measured before and after the LISN. The 50 Hz mains voltage remains unchanged in magnitude and phase.

Figure 8: Performance of the designed LISN.
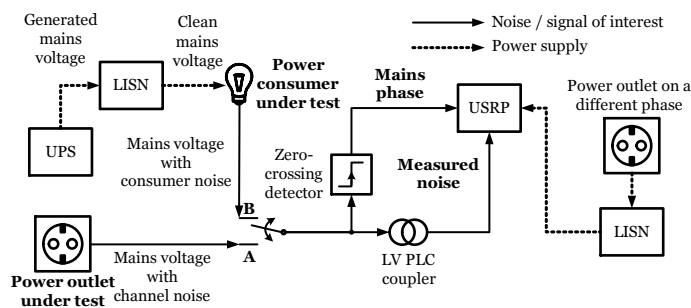
Figure 9: The power line noise measuring setup. When the switch is set to A, the channel noise is measured; when switched to B, the consumer noise is measured.

(a) Channel noise at an power outlet in office.
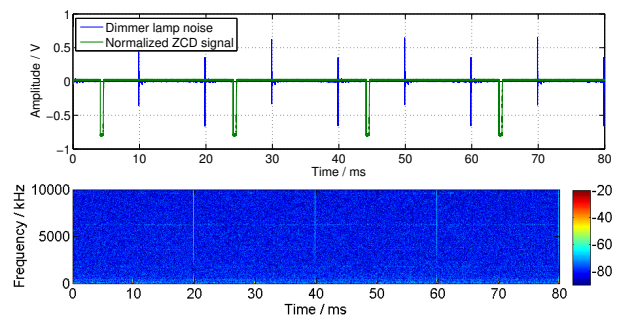
(b) Noise generated by a dimmer.
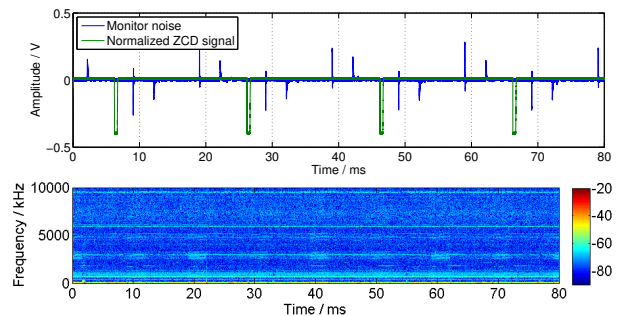
(c) Noise generated by a monitor.

Figure 10: Three laboratory noise measurements.

Table IV: Estimated parameters of the PIN in the laboratory channel measurement.

$\Delta\tau$ (ms)	τ_w (µs)	τ_0 (µs)	A
10	40	5200	0.2

NBNs, which may be caused by the synchronizing signals for its communication with the computer.

We applied our characterization approach to the channel noise measurement in Fig. 10a for a case study, because it shows a more complicated behavior than both consumer measurements. A strong periodical NBN was detected at 16.16 kHz with a bandwidth of 1 kHz. The estimated 100 Hz

envelope is shown in Fig. 11. A PIN synchronous to the mains was extracted, the parameters of which are listed in Table IV. No APIN was detected in the measurement. Ten different filters were estimated for the time-varying CBGN, as shown in Fig. 12.

Then we emulated the measured channel noise with our emulator. The spectrogram is shown in Fig. 13. The charac-
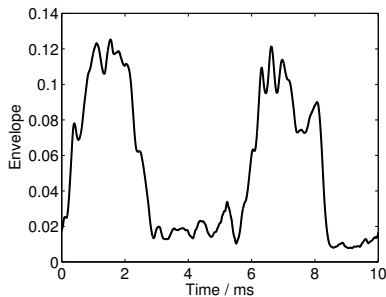
Figure 11: Estimated envelope of the NBN in the laboratory channel measurement, amplitude normalized to a WGN with unity gain.
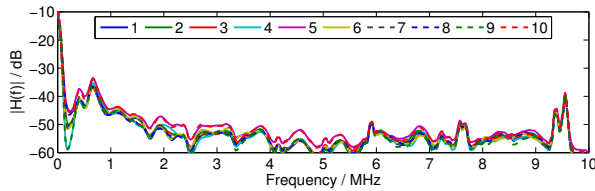
Figure 12: The transfer functions of the ten estimated CBGN filters.

teristics in the frequency domain and time domain were reconstructed. Note that the noise at lower frequencies, i.e. below $150\,\mathrm{kHz}$, including the NBNs, appears strongly attenuated in the emulation, due to the frequency response of the amplifier of the emulator, which was designed for the frequency band between 0.15 and $10\,\mathrm{MHz}$.

VI. CONCLUSION AND OUTLOOKS

In this paper, aiming at the frequency band from 0.15 to $10\,\mathrm{MHz}$, we reviewed the existing models of power line noise. For every known noise category, we selected a model and proposed an approach of extraction and parameterization. The methods were tested with synthesized noise. Based on the selected models, we designed and implemented an FPGA-based real time noise emulator, which can regenerate a noise scenario according to the estimated noise parameters. We also designed a measuring system which can capture the noises of both LV power line channels and power consumers. A laboratory channel noise measurement was analyzed with our
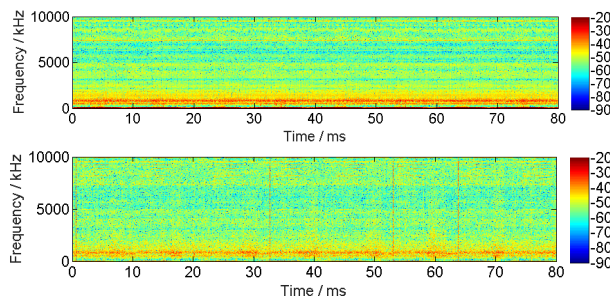
Figure 13: The PSD of the measured (top) and emulated (bottom) channel noises over time, in dBV^2

characterizing methods and emulated with our emulator. The emulation was then compared to the measurement to validate the emulation. As future work, other properties of LV power line channels such as the transfer function and the access impedance shall be characterized and emulated as well.

REFERENCES

[1] Stefano Galli, Anna Scaglione, and Zhifang Wang, "For the grid and through the grid: The role of power line communications in the smart grid," *Proceedings of the IEEE*, vol. 99, no. 6, pp. 998–1027, 2011.
[2] Manfred Zimmermann and Klaus Dostert, "An analysis of the broadband noise scenario in powerline networks," in *International Symposium on Powerline Communications and its Applications (ISPLC2000)*, 2000, pp. 5–7.
[3] Matthias Götz, Manuel Rapp, and Klaus Dostert, "Power line channel characteristics and their effect on communication system design," *Communications Magazine*, vol. 42, no. 4, pp. 78–86, 2004.
[4] José Antonio Cortés, Luis Diez, Francisco Javier Canete, and Juan José Sánchez-Martínez, "Analysis of the indoor broadband power-line noise scenario," *Transactions on Electromagnetic Compatibility*, vol. 52, no. 4, pp. 849–858, 2010.
[5] Wenqing Liu, Martin Sigle, and Klaus Dostert, "Channel characterization and system verification for narrowband power line communication in smart grid applications," *Communications Magazine, IEEE*, vol. 49, no. 12, pp. 28–35, 2011.
[6] Pascal pagani, Rehan Hashmat, Andreas Schwager, Daniel Schneider, and W Baschlin, "European mimo plc field measurements: Noise analysis," in *International Symposium on Power Line Communications and its Applications (ISPLC)*. IEEE, 2012, pp. 310–315.
[7] Pascal, Andreas Schwager, Piet Janse Van Rensburg, et al., "Introduction to power line communication channel and noise characterisation," pp. 3–37, 2014.
[8] FJ Cañete, L Diez, JA Cortés, JJ Sánchez-Martínez, and Luis M Torres, "Time-varying channel emulator for indoor power line communications," in *Proceedings of the 51th Annual IEEE Global Telecommunications Conference (GLOBECOM)*, 2008, pp. 1–5.
[9] Nico Weling, "Flexible fpga-based powerline channel emulator for testing mimo-plc, neighborhood networks, hidden node or vdsl coexistence scenarios," in *International Symposium on Power Line Communications and its Applications (ISPLC)*. IEEE, 2011, pp. 12–17.
[10] Nico Weling, Andreas Engelen, and Stephan Thiel, "Broadband mimo powerline channel emulator," in *International Symposium on Power Line Communications and its Applications (ISPLC)*. IEEE, 2014, pp. 105–110.
[11] Nico Weling, Andreas Engelen, and Stephan Thiel, "Broadband mimo powerline channel emulator verication and testing results," in *International Symposium on Power Line Communications and its Applications (ISPLC)*. IEEE, 2015, pp. 59–64.
[12] Wenqing Liu, *Emulation of Narrowband Powerline Data Transmission Channels and Evaluation of PLC Systems*, KIT Scientific Publishing, Karlsruhe, 2013.
[13] Weilin Liu, Gerd Bumiller, and Hongjian Gao, "On (power-) line defined plc system," in *International Symposium on Power Line Communications and its Applications (ISPLC)*. IEEE, 2014, pp. 81–86.
[14] Klaus Dostert, *Powerline Communications*, Prentice Hall PTR, 2001.
[15] Morgan HL Chan and Robert W Donaldson, "Amplitude, width, and interarrival distributions for noise impulses on intrabuilding power line communication networks," *Transactions on Electromagnetic Compatibility*, vol. 31, no. 3, pp. 320–323, 1989.
[16] H Meng, Y Ll Guan, and S Chen, "Modeling and analysis of noise effects on broadband power-line communications," *Transactions on Power Delivery*, vol. 20, no. 2, pp. 630–637, 2005.
[17] Mohamed Tlich, Hassina Chaouche, Ahmed Zeddam, and Pascal Pagani, "Novel approach for plc impulsive noise modelling," in *International Symposium on Power Line Communications and its Applications (ISPLC)*. IEEE, 2009, pp. 20–25.
[18] Fabio Gianaroli, Fabrizio Pancaldi, Enrico Sironi, Marco Vigilante, Giorgio Matteo Vitetta, and Alessandro Barbieri, "Statistical modeling of periodic impulsive noise in indoor power-line channels," *Transactions on Power Delivery*, vol. 27, no. 3, pp. 1276–1283, 2012.
[19] Luca Di Bert, Peter Caldera, David Schwingshackl, and Andrea M Tonello, "On noise modeling for power line communications," in *International Symposium on Power Line Communications and its Applications (ISPLC)*. IEEE, 2011, pp. 283–288.

[20] Hassina Chaouche, Frederic Gauthier, Ahmed Zeddam, Mohamed Tlich, and Mohamed Machmoum, "Time domain modeling of powerline impulsive noise at its source," *Journal of Electromagnetic Analysis and Applications*, vol. 2011, 2011.

[21] Massimo Antoniali, Fabio Versolatto, and Andrea Tonello, "An experimental characterization of the plc noise at the source," *Transactions on Power Delivery*, vol. PP, no. 99, pp. 1–1, 2015.

[22] Deniz Rende, Arun Nayagam, Kaywan Afkhamie, Larry Yonge, Raffaele Riva, Daniele Veronesi, Fabio Osnato, and Paola Bisaglia, "Noise correlation and its effect on capacity of inhome mimo power line channels," in *International Symposium on Power Line Communications and its Applications (ISPLC)*. IEEE, 2011, pp. 60–65.

[23] Tech. Rep. (TR) European Telecommunication Standardization Institute (ETSI), "101 562-3 v 1.1. 1,powerline telecommunications (plt); mimo plt; part 3: Setup and statistical results of mimo plt channel and noise measurements,," Tech. Rep., 2012.

[24] Alberto Pittolo, Andrea M Tonello, and Fabio Versolatto, "Performance of mimo plc in measured channels affected by correlated noise," in *International Symposium on Power Line Communications and its Applications (ISPLC)*. IEEE, 2014, pp. 261–265.

[25] Olaf G Hooijen, "A channel model for the residential power circuit used as a digital communications medium," *IEEE Transactions on Electromagnetic Compatibility*, vol. 40, no. 4, pp. 331–336, 1998.

[26] Manfred Zimmermann and Klaus Dostert, "Analysis and modeling of impulsive noise in broad-band powerline communications," *IEEE Transactions on Electromagnetic Compatibility*, vol. 44, no. 1, pp. 249–258, 2002.

[27] Manfred Zimmermann, *Energieverteilnetze als Zugangsmedium für Telekommunikationsdienste*, Shaker, 2000.

[28] Karl F Nieman, Jing Lin, Mohamed Nassar, Khurram Waheed, and Brian L Evans, "Cyclic spectral analysis of power line noise in the 3–200 khz band," in *International Symposium on Power Line Communications and its Applications (ISPLC)*.

[29] Klaus Dostert, Martin Sigle, and Wenqing Liu, "Narrowband characterisation in an office environment," pp. 39–68, 2014.

[30] Masaaki Katayama, Takaya Yamazato, and Hiraku Okada, "A mathematical model of noise in narrowband power line communication systems," *Journal on Selected Areas in Communications*, vol. 24, no. 7, pp. 1267–1276, 2006.

[31] Marcel Nassar, Anand Dabak, Il Han Kim, Tarkesh Pande, and Brian L Evans, "Cyclostationary noise modeling in narrowband powerline communication for smart grid applications," in *International Conference on Acoustics, Speech and Signal Processing (ICASSP)*. IEEE, 2012, pp. 3089–3092.

[32] Aryan Saadat Mehr and Tongwen Chen, "Properties of linear switching time-varying discrete-time systems with applications," *Systems & Control Letters*, vol. 39, no. 4, pp. 229–235, 2000.

[33] S. Sancha, F. J. Canete, L Diez, and J. T. Entrambasaguas, "A channel simulator for indoor power-line communications," in *International Symposium on Power Line Communications and Its Applications (ISPLC)*. IEEE, 2007, pp. 104–109.

[34] Jörg Bausch, Timo Kistner, Marko Babic, and Klaus Dostert, "Characteristics of indoor power line channels in the frequency range 50-500 khz," in *International Symposium on Power Line Communications and its Applications (ISPLC)*. IEEE, 2006, pp. 86–91.

[35] Oliver Opalko, Martin Sigle, and Klaus Dostert, "Detection of am broadcasting stations on low voltage power lines," in *International Symposium on Power Line Communications and its Applications (ISPLC)*. IEEE, 2014, pp. 87–92.

[36] Bin Han, Cornelius Kaiser, and Klaus Dostert, "A novel approach of canceling cyclostationary noises in low-voltage powerline communications," in *International Conference on Communications (ICC)*. 2015, IEEE.

[37] Osamu Ohno, Masaaki Katayama, Takaya Yamazato, and Akira Ogawa, "A simple model of cyclostationary power-line noise for communication systems," in *International Symposium on Power Line Communications and its Applications (ISPLC)*, 1998, pp. 115–122.

[38] Masaaki Katayama, Saori Itou, Takaya Yamazato, and Akira Ogawa, "Modeling of cyclostationary and frequency dependent power-line channels for communications," in *International Symposium on Power Line Communication and its Applications (ISPLC*, 2000, pp. 123–130.

[39] Masaaki Katayama, Takaya Yamazato, and Hiraku Okada, "A mathematical model of narrowband power-line noise based on measurements," in *International Symposium on Power Line Communications and its Applications (ISPLC)*, 2005.

[40] Matthias Götz, *Mikroelektronische, echtzeitfähige Emulation von Powerline-munikationskanälen*, Mensch & Buch Verlag, Berlin, 2004.

[41] Jing Lin and Brian L Evans, "Cyclostationary noise mitigation in narrowband powerline communications," in *Asia-Pacific Signal & Information Processing Association Annual Summit and Conference (APSIPA ASC)*. IEEE, 2012, pp. 1–4.

[42] David Middleton, "Procedures for determining the parameters of the first-order canonical models of class a and class b electromagnetic interference," *Transactions on Electromagnetic Compatibility*, , no. 3, pp. 190–208, 1979.

[43] Hendrik C Ferreira, Henricus M Grové, Olaf Hooijen, and AJ Han Vinck, *Power Line Communication*, Wiley Online Library, 2001.

[44] Marcel Nassar, Jing Lin, Yousof Mortazavi, Anand Dabak, Il Han Kim, and Brian L Evans, "Local utility power line communications in the 3–500 khz band: Channel impairments, noise, and standards," *Signal Processing Magazine*, vol. 29, no. 5, pp. 116–127, 2012.

[45] Jing Lin, Mohamed Nassar, and Brian L Evans, "Impulsive noise mitigation in powerline communications using sparse bayesian learning," *Journal on Selected Areas in Communications*, vol. 31, no. 7, pp. 1172–1183, 2013.

[46] Monisha Ghosh, "Analysis of the effect of impulse noise on multicarrier and single carrier qam systems," *IEEE Transactions on Communications*, vol. 44, no. 2, pp. 145–147, 1996.

[47] Riccardo Pighi, Michele Franceschini, Gianluigi Ferrari, and Riccardo Raheli, "Fundamental performance limits of communications systems impaired by impulse noise," *IEEE Transactions on Communications*, vol. 57, no. 1, pp. 171–182, 2009.

[48] Yang Lu, Weilin Liu, Jianqi Li, and Hongjian Gao, "Measurement and cognitive detection method of broadcast radio stations in distribution networks," in *International Symposium on Power Line Communications and its Applications (ISPLC)*. IEEE, 2014, pp. 75–80.

[49] F. Bonnardot, R. B. Randall, and F. Guillet, "Extraction of second-order cyclostationary sourcesapplication to vibration analysis," *Mechanical Systems and Signal Processing*, vol. 19, no. 6, pp. 1230–1244, 2005.

[50] William A Gardner, Antonio Napolitano, and Luigi Paura, "Cyclostationarity: Half a century of research," *Signal Processing*, vol. 86, no. 4, pp. 639–697, 2006.

[51] Martin Sigle, Wenqing Liu, and Klaus Dostert, "On the impedance of the low-voltage distribution grid at frequencies up to 500 khz," in *International Symposium on Power Line Communications and its Applications (ISPLC)*. IEEE, 2012, pp. 30–34.

[52] Mengling Feng, Liang Yu Loy, Feng Zhang, and Cuntai Guan, "Artifact removal for intracranial pressure monitoring signals: a robust solution with signal decomposition," in *Annual International Conference of the IEEE Engineering in Medicine and Biology Society, EMBC*. IEEE, 2011, pp. 797–801.

[53] Mengling Feng, Liang Yu Loy, Kihong Sim, Clifton Phua, Feng Zhang, and Cuntai Guan, "Artifact correction with robust statistics for non-stationary intracranial pressure signal monitoring," in *International Conference on Pattern Recognition (ICPR)*. IEEE, 2012, pp. 557–560.

[54] Bin Han, Michael Muma, Mengling Feng, and Abdelhak M Zoubir, "An online approach for intracranial pressure forecasting based on signal decomposition and robust statistics," in *International Conference on Acoustics, Speech and Signal Processing (ICASSP)*. IEEE, 2013, pp. 6239–6243.

[55] Norden E Huang, Zheng Shen, Steven R Long, Manli C Wu, Hsing H Shih, Quanan Zheng, Nai-Chyuan Yen, Chi Chao Tung, and Henry H Liu, "The empirical mode decomposition and the hilbert spectrum for nonlinear and non-stationary time series analysis," in *Proceedings of the Royal Society of London A: Mathematical, Physical and Engineering Sciences*. The Royal Society, 1998, vol. 454, pp. 903–995.

[56] George EP Box, Gwilym M Jenkins, and Gregory C Reinsel, *Time Series Analysis: Forecasting and Control*, vol. 734, John Wiley & Sons, 2011.

[57] Abdelhak M Zoubir, Visa Koivunen, Yacine Chakhchoukh, and Michael Muma, "Robust estimation in signal processing: A tutorial-style treatment of fundamental concepts," *Signal Processing Magazine*, vol. 29, no. 4, pp. 61–80, 2012.

www.kit.edu